Supplementary Information for "Tuning the Ultrafast Response of Fano Resonances in Halide Perovskite Nanoparticles"

Paolo Franceschini,[*,†,‡,¶] Luca Carletti,[*,§,‖] Anatoly P. Pushkarev,[⊥] Fabrizio Preda,[#,@] Antonio Perri,[#,@] Andrea Tognazzi,[‖,△] Andrea Ronchi,[†,‡,¶] Gabriele Ferrini,[†,‡] Stefania Pagliara,[†,‡] Francesco Banfi,[▽] Dario Polli,[#,@] Giulio Cerullo,[#] Costantino De Angelis,[‖,△] Sergey V. Makarov,[⊥] and Claudio Giannetti[*,†,‡]

†*Department of Mathematics and Physics, Università Cattolica del Sacro Cuore, Brescia I-25121, Italy*

‡*ILAMP (Interdisciplinary Laboratories for Advanced Materials Physics), Università Cattolica del Sacro Cuore, Brescia I-25121, Italy*

¶*Department of Physics and Astronomy, KU Leuven, Celestijnenlaan 200D, 3001 Leuven, Belgium*

§*Department of Information Engineering, University of Padova, Padova 35131, Italy*

‖*Department of Information Engineering, University of Brescia, Brescia 25123, Italy*

⊥*ITMO University, Saint Petersburg 197101, Russia*

#*Dipartimento di Fisica, Politecnico di Milano, Milano 20133, Italy*

@*NIREOS S.R.L., Via G. Durando 39, 20158 Milano, Italy (www.nireos.com)*

△*National Institute of Optics (INO), Consiglio Nazionale delle Ricerche (CNR), Brescia 25123, Italy*

▽*FemtoNanoOptics group, Université de Lyon, CNRS, Université Claude Bernard Lyon 1, Institut Lumière Matière, F-69622 Villeurbanne, France*

E-mail: paolo.franceschini@unicatt.it; luca.carletti@unibs.it; claudio.giannetti@unicatt.it

S1 Supplementary Figure

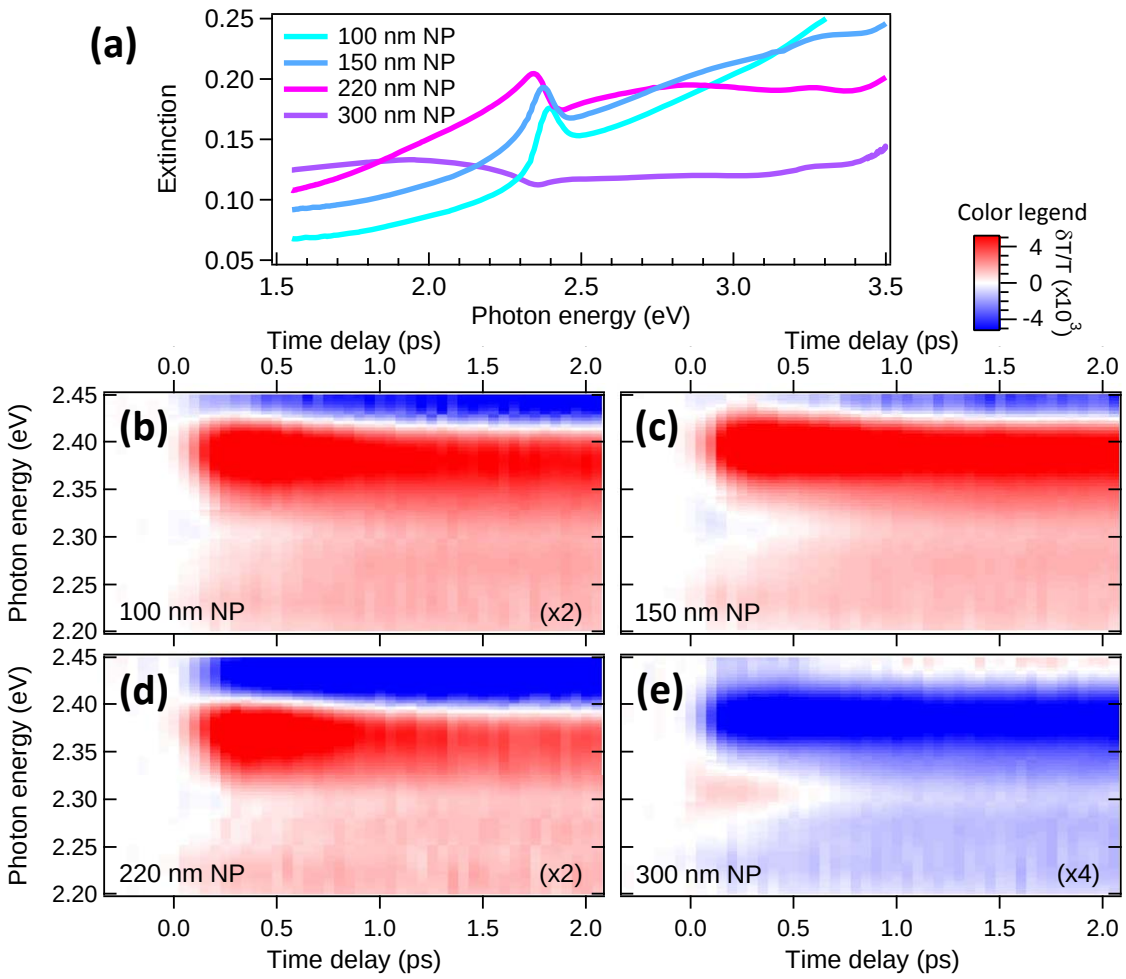

Figure S1: (a) Equilibrium extinction spectra of $CsPbBr_3$ NPs of different size. (b-e) Time- and energy-resolved $\delta T/T$ maps corresponding to the NPs whose extinction is reported in panel (a).

S2 Effective medium theory and model for the differential transmission

In Fig. 1 (main text) we show the fit of the Fano profile (Eq. 1 of the main text) to the experimental extinction (X) of the 150 and 300 nm NP samples at equilibrium. In Eq. 1 of the main text, $X_{\rm bck}$ accounts for the absorption across the semiconducting edge and its analytical expression is given by a second-order polynomial function

$$X_{\rm bck}(\hbar\omega) = k_0 + k_1 \cdot (\hbar\omega) + k_2 \cdot (\hbar\omega)^2, \tag{S1}$$

where k_0, k_1, and k_2 are free parameters.

Given the relation $X = -\log_{10} T$ (where T is the sample transmission), it follows that the differential transmission ($\delta T/T$) is:

$$\frac{\delta T}{T} = 10^{-\delta X} - 1 \simeq -\frac{1}{\log_{10} e}\delta X, \tag{S2}$$

where δX is the differential extinction.

Fig. S2a displays the experimental $\delta T/T$ spectra of the 150 nm NP sample, taken at delay time $\Delta t = 2$ ps. The experimental data (circles) can be reproduced (solid line) by assuming a blue-shift $\delta E_g = (5.1 \pm 0.4)$ meV of the Fano profile (Eq. 1 of the main text). As discussed in the main text, the observed blue-shift δE_g refers to the whole sample, which can be modelled as an effective medium consisting in $CsPbBr_3$ nanoparticles surrounded by air. To compare the measured band-gap shift (δE_g) to the values reported in literature for thin films of similar perovskite compounds, we adopt the Modified Maxwell-Garnett Mie model (MMGM),[1] which accounts for the geometry dispersion of Mie resonators, to extract a scaling factor $\tilde{C}$. This scaling factor allows us to estimate the intrinsic bandgap shift of individual nanoparticles (δE_g^{NP}) and compare it to results obtained on thin films.

According to the MMGM model, the dielectric function of the effective medium ($\varepsilon_{\rm eff}$) is

related to that of the nanoparticles ($\varepsilon_{\rm np}$) and of the surrounding medium ($\varepsilon_{\rm m}$) through the relation:

$$\frac{\varepsilon_{\rm eff}-\varepsilon_{\rm m}}{\varepsilon_{\rm eff}+2\varepsilon_{\rm m}}=\frac{3if_{\rm vol}}{2}\left(\frac{\lambda_0}{\pi\sqrt{\varepsilon_{\rm m}}\,\bar{\phi}}\right)^3\int_{\phi_1}^{\phi_2}\mathcal{F}(\phi)\;a_1(\phi;\lambda_0)\;{\rm d}\phi \tag{S3}$$

where $f_{\rm vol}$ is the volume fraction of the inclusion (see Sec. S2.1 for the details of the calculation), λ_0 is the wavelength in vacuum, $\bar{\phi}$ is the average diameter of the NPs, $\mathcal{F}(\phi)$ is the NPs diameter distribution function, ϕ_1 and ϕ_2 are the lower and upper limits of the size distribution. The term $a_1(\phi;\lambda)$ is the *first electric* (see Sec. S6.2 for more details) Mie coefficient given by:

$$a_1(\phi;\lambda_0)=\frac{\sqrt{\varepsilon_{\rm np}}\,\psi_1\big(\pi\phi\sqrt{\varepsilon_{\rm np}}/\lambda_0\big)\,\psi_1'\big(\pi\phi\sqrt{\varepsilon_{\rm m}}/\lambda_0\big)-\sqrt{\varepsilon_{\rm m}}\,\psi_1\big(\pi\phi\sqrt{\varepsilon_{\rm m}}/\lambda_0\big)\,\psi_1'\big(\pi\phi\sqrt{\varepsilon_{\rm np}}/\lambda_0\big)}{\sqrt{\varepsilon_{\rm np}}\,\psi_1\big(\pi\phi\sqrt{\varepsilon_{\rm np}}/\lambda_0\big)\,\xi_1'\big(\pi\phi\sqrt{\varepsilon_{\rm m}}/\lambda_0\big)-\sqrt{\varepsilon_{\rm m}}\,\xi_1\big(\pi\phi\sqrt{\varepsilon_{\rm m}}/\lambda_0\big)\,\psi_1'\big(\pi\phi\sqrt{\varepsilon_{\rm np}}/\lambda_0\big)}, \tag{S4}$$

where ψ and ξ are the Riccati - Bessel functions. We assume that the equilibrium dielectric function of the nanoparticle $\varepsilon_{\rm np}$ equals that of the $CsPbBr_3$ thin film (which is extracted from Ref. 2). According to the experimental distribution of the NPs diameters reported in Fig. 1 of the main text, we assume a normal distribution of diameters given by: $\mathcal{F}(\phi)=1/\sqrt{2\pi\sigma_\phi^2}\;e^{-\left(\frac{\phi-\bar{\phi}}{\sqrt{2}\,\sigma_\phi}\right)^2}$, where σ_ϕ is the standard deviation of the distribution. In the case of the 150 nm NPs sample, $\bar{\phi}=150\,{\rm nm}$ and $\sigma_\phi=17\,{\rm nm}$.

Within the framework of MMGM theory, we calculated the scaling factor $\tilde{C}$ as the ratio between the absorption[1] variation of the nanoparticles ($\delta\alpha_{\rm np}$) and the absorption variation of the sample ($\delta\alpha_{\rm eff}$), *i.e.* $\tilde{C}{=}\delta\alpha_{\rm np}/\delta\alpha_{\rm eff}$. Fig. S2b reports the comparison between the variation of the absorption coefficient of the sample $\delta\alpha_{\rm eff}$ (yellow solid line) and of the nanoparticles $\delta\alpha_{\rm np}$ (black solid line). To calculate $\tilde{C}$ we optimize the overlap between the absorption

[1]The absorption coefficient α is related to the dielectric function $\varepsilon=\varepsilon^{(1)}+i\varepsilon^{(2)}$ via

$$\alpha=\frac{2\omega}{c}\sqrt{\frac{-\varepsilon^{(1)}+\sqrt{\left(\varepsilon^{(1)}\right)^2+\left(\varepsilon^{(2)}\right)^2}}{2}},$$

where ω is the optical frequency and c the velocity of light in vacuum.

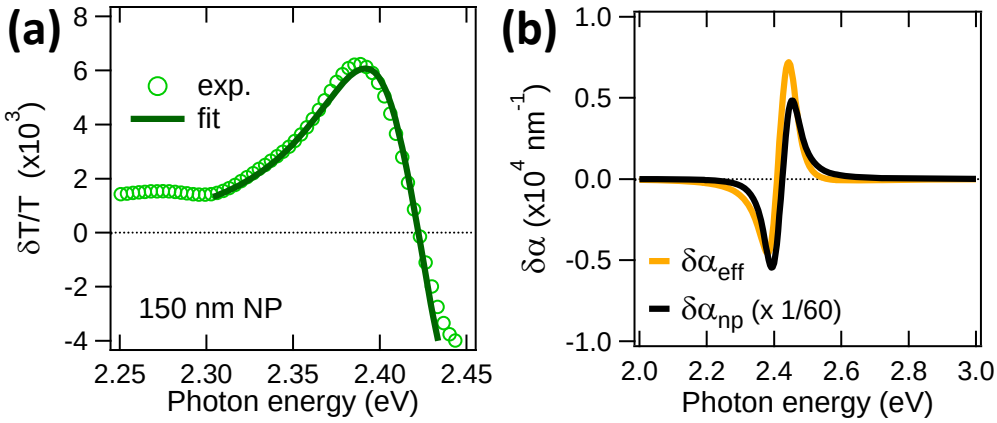

Figure S2: **Out-of-equilibrium properties at long time delays.** (a) Experimental differential transmission spectra (green markers) for 150 nm nanoparticles, taken at $\Delta t = 2\,\mathrm{ps}$ after excitation. The solid line is obtained by fitting Eq. S2 to the experimental data in the energy region near the resonance. (b) Variation of the absorption coefficient of the effective medium $\delta\alpha_{\mathrm{eff}}$ (yellow solid line) and of the inclusion $\delta\alpha_{\mathrm{np}}$ (black solid line); the latter is multiplied by a factor 1/60.

variations at energies smaller than the exciton peak, which is the region investigated by our pump-probe experiment. Following this procedure we obtain $\tilde{C}= (60 \pm 40)$. The error is calculated taking into account the fact that the samples consist in lattices of randomly distributed nanoparticles. The average coverage distribution density is $\sigma_{cov} = 3$ NP/μm^2, but it oscillates in the range $1 \div 5$ NP/μm^2.

S2.1 Calculation of the volume fraction f_{vol}

The volume fraction f_{vol} can is estimated as (see Fig. S3):

$$f_{vol} = \frac{V \cdot N}{V_{tot}} = \frac{\frac{4}{3}\pi\left(\frac{\bar{\phi}}{2}\right)^3 \cdot \sigma_{cov} \cdot S}{\bar{\phi} \cdot S} = \frac{\pi}{6} \cdot \sigma_{cov} \cdot \bar{\phi}^2,$$

where V is the volume of the single nanoparticle, V_{tot} is the volume of the selected region (the height of the cylinder equals the mean nanoparticle diameter), N number of particles within the selected region, $\bar{\phi}$ is the mean nanoparticle diameter, σ_{cov} is the average coverage distribution density, and S is area of the base of the selected region. Considering the experimental parameters $\bar{\phi} = 150\,\text{nm}$ and $\sigma_{cov} = 3\ \text{NP}/\mu\text{m}^2$, it follows that $f_{vol} = 0.035$.

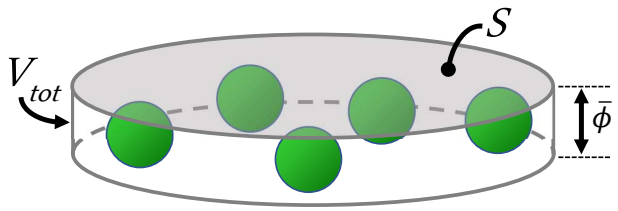

Figure S3: **Calculation of the volume fraction f_{vol}.** Sketch of the region adopted to estimate the volume fraction. V_{tot} is the volume of the selected region (gray solid line), S is area of the base of the selected region (shadowed gray surface), and $\bar{\phi}$ is mean nanoparticle diameter. The height of the cylinder equals the mean nanoparticle diameter.

S3 Calculation of the pump photon density

The initial free-carrier density injected by each pump pulse has been evaluated by taking into account the material extinction, the fluence employed in the pump-probe experiment, and the structural properties of the nanoparticles. The incident fluence is $F = 54\,\mu\mathrm{J/cm^2}$ at $\lambda = 425\,\mathrm{nm}$. For 150 nm NPs, the extinction at the pump wavelength is $X = 0.207$ and the equilibrium transmission results equal to $T = 10^{-X} = 0.63$. Taking into account the reflection from the substrate (R=0.08) and assuming that the energy is absorbed by the nanoparticles, the absorption due to the nanoparticles is $A = 1 - (R + T) = 0.29$. It follows that the absorbed fluence is $E_{\mathrm{A}} = F \cdot A = 15.5\,\mu\mathrm{J/cm^2}$ and, therefore, the energy absorbed over an area $\mathcal{A} = 1\,\mu\mathrm{m^2}$ is $E_{\mathrm{a}} = E_{\mathrm{A}} \cdot \mathcal{A} = 1.55 \times 10^{-13}\,\mathrm{J}$. Given an average coverage distribution density of $\sigma_{cov} = 3\,\mathrm{NP}/\mu\mathrm{m^2}$ and assuming a spherical shape for the nanoparticles, which gives a volume $V = 1.767 \times 10^{-15}\,\mathrm{cm^3}$, the energy absorbed per unit volume is $w_{\mathrm{a}} = E_{\mathrm{a}}/(3 \cdot V) = 29.2\,\mathrm{Jcm^{-3}} = 1.82 \times 10^{20}\,\mathrm{eVcm^{-3}}$. Finally, given that the pump is centered at $\lambda = 425\,\mathrm{nm}$, the photon density per unit volume at the pump wavelength is $n_{ph} = 62.6 \times 10^{18}\,\mathrm{cm^{-3}}$.

S4 Analysis of the time-resolved traces

The time-resolved $\delta T/T(\Delta t)$ traces, at fixed probe energy, are analysed according to the following double-exponential model. This choice is due to the fact that we want to describe the dynamics of the differential signal as the sum of the contributions due to *bandgap renormalization* (BGR) and *band filling* (BF). The $\delta T/T(\Delta t)$ model is given by the convolution between a gaussian function $\mathcal{G}$, describing the experimental time resolution (given by the pump temporal width), and the material response function $\mathcal{F}$:

$$\delta T/T(\Delta t) = \mathcal{G}(\Delta t) * \mathcal{F}(\Delta t)\,, \qquad \text{where} \qquad \mathcal{G}(t) = \sqrt{\frac{4\,\ln 2}{\pi\,\tau_p^2}}\, e^{-\frac{4\,\ln 2}{\tau_p^2}\,t^2} \qquad \text{and} \tag{S5}$$

$$\mathcal{F}(\Delta t) = \theta(\Delta t - t_0)\cdot\Big[A_1\cdot\Big(1-e^{-\frac{\Delta t-t_0}{\tau_{R1}}}\Big)\cdot e^{-\frac{\Delta t-t_0}{\tau_{D1}}} + \\ + A_2\cdot\Big(1-e^{-\frac{\Delta t-t_0}{\tau_{R2}}}\Big)\cdot e^{-\frac{\Delta t-t_0}{\tau_{D2}}}\Big]\,. \tag{S6}$$

In the previous expressions, τ_p=40 fs is the FWHM of the pump-laser pulse, t_0 is the zero-time offset, τ_{R1} is the BGR rise time, τ_{D1} is the BGR decay time, τ_{R2} is the BF rise time, τ_{D2} is the BF decay time, A_1 and A_2 are the amplitude factors of the two mechanisms.

Table S1: Parameters extracted from the fit procedure applied to the $\delta T/T$ dynamics at different probe energies

Parameter	150-nm-NP	300-nm-NP
τ_{R1} (fs)	200 ± 10	190 ± 10
τ_{D1} (fs)	410 ± 10	390 ± 10
τ_{R2} (fs)	500 ± 20	460 ± 20

S5 Models of the dynamics of the single nanoparticle optical properties

Here, we report the description of the models adopted to establish the role of the different physiscal phenomena in determining the out-of-equilibrium optical properties of the single nanoparticle. Upon free-carriers injection, the transmission variation is controlled by three main components:[3] the Drude term (D), the band filling (BF) and the bandgap renormalization (BGR) effects. These processes give rise to a modulation of both the refractive index and absorption, as given by:

$$\delta n = \delta n_D + \delta n_{BGR} + \delta n_{BF} \tag{S7a}$$

$$\delta \alpha = \delta \alpha_D + \delta \alpha_{BGR} + \delta \alpha_{BF} \tag{S7b}$$

For each process (i=D, BGR, BF), the refractive index and absorption variations are constrained by the following Kramers-Krönig relations:

$$\delta n_i(\hbar\omega; n_{fc}) = \frac{2c\hbar}{e^2}\ \text{P.V.} \int_0^{+\infty} \frac{\delta \alpha_i(\xi; n_{fc})}{\xi^2 - (\hbar\omega)^2}\, \mathrm{d}\xi, \tag{S8}$$

where c is the speed of light in vacuum, e is the electron charge, $\hbar$ is the Planck's constant, and *P.V.* is the Cauchy principal value.[3,4] As it will be described in the following, these three components depend on the pump-injected free-carriers density n_{fc}. In our analysis, we assume an injected free-carrier density $n_{fc} = 1.2 \times 10^{20}\,\mathrm{cm}^{-3}$ for 150 nm NPs; moreover, the pump-injected free-electron density in the conduction band (n_e) is assumed equal to the pump-injected free-holes density in the valence band (n_h), *i.e.* $n_e \simeq n_h \simeq n_{fc}/2$.

S5.1 Drude

The Drude term represents the physical mechanism for which the photon-absorption promotes a free-carrier to a higher energy state within the same band. The corresponding change in the refractive index is given by:

$$\delta n_D\left(E; n_{fc}\right) = -\frac{n_{fc}\,\hbar^2\,e^2}{4\,m^*\,n_0\,\varepsilon_0\,\left(E^2+\hbar^2\,\gamma^2\right)}, \tag{S9}$$

where $m^* = \left(m_e^{-1}+m_h^{-1}\right)^{-1}$ is the reduced-effective mass ($m^* = 0.072\,m_0$,[5]), n_0 is the refractive index at equilibrium and γ is the inverse collision time of the carriers.

S5.2 Bandgap Renormalization

In the case of parabolic bands, the optical absorption (α_0) of electrons (holes) from the valence (conduction) band to the conduction (valence) band is given by the square-root law:

$$\alpha_{eq}\left(\hbar\omega; E_g^0\right) = \begin{cases} 0 & \text{for } \hbar\omega < E_g^0, \\ \frac{C_1}{\hbar\omega}\sqrt{\hbar\omega - E_g} + C_2\,\frac{\Gamma/2}{\left[\hbar\omega-\left(E_g^0-E_x\right)\right]^2+(\Gamma/2)^2} & \text{for } \hbar\omega \geq E_g^0 \end{cases}, \tag{S10}$$

where E_g^0, E_x, and C are respectively the band-gap energy, the exciton binding energy and a constant. The bandgap renormalization term is modeled as a rigid translation (red shift) of the absorption curve:

$$\delta\alpha_{BGR}(\hbar\omega; n_{fc}/n_{cr}) = \alpha_{eq}\left(\hbar\omega; E_g^0 - \delta E_{BGR}(n_{fc}/n_{cr})\right) - \alpha_{eq}\left(\hbar\omega; E_g^0\right), \tag{S11}$$

where δE_{BGR} is the free-carrier dependent bandgap shift, whose expression is

$$\delta E_{BGR}(n_{fc}/n_{cr}) = \begin{cases} \frac{C_3}{\varepsilon_s}\left(1-\frac{n_{fc}}{2\,n_{cr}}\right)^{1/3}, & n_{fc}/2 \geq n_{cr} \\ 0, & n_{fc}/2 < n_{cr} \end{cases}, \tag{S12}$$

where C_3=0.05 is a fitting parameter, ε_s= 4 (Ref. 6) is the relative static dielectric constant, and n_{cr} is the critical concentration of free carriers,[3] which is calculated as

$$n_{cr}\left[\mathrm{cm}^{-3}\right] = \left(\frac{m^*/m_0}{1.4\,\varepsilon_s}\right)^3 \cdot 1.6\times 10^{24} = 3.4\times 10^{18}. \tag{S13}$$

S5.3 Band Filling

The band filling term implies a free-carriers induced modulation of the interband absorption for photon energies slightly above the nominal bandgap. In presence of free-carriers injection, the variation of the intraband absorption is described by the following expression:

$$\delta\alpha_{BF}(\hbar\omega; n_{fc}, T^*) = \alpha_{eq}\big(\hbar\omega; E_g^0\big)\ \left[f_v\big(\hbar\omega; E^*_{F_v}, T^*\big) - f_c\big(\hbar\omega; E^*_{F_c}, T^*\big) - 1\right], \tag{S14}$$

where

$$f_v\big(\hbar\omega; E^*_{F_v}, T^*\big) = \left[1+\exp\left(\frac{E_a - E^*_{F_v}}{k_B T^*}\right)\right]^{-1} \text{and } f_c\big(\hbar\omega; E^*_{F_c}, T^*\big) = \left[1+\exp\left(\frac{E_b - E^*_{F_c}}{k_B T^*}\right)\right]^{-1} \tag{S15}$$

are the Fermi-Dirac distributions for the electrons in the conduction band and holes in the valence band, respectively. In Eq. S15, T^* is the effective temperature, E_a and E_b denote an energy level in the valence and conduction band, and $E^*_{F_v}$ and $E^*_{F_c}$ are the carrier-dependent quasi-Fermi levels. The effective temperature T^* is computed by considering the excess energy of the pump-excited free-carriers which, in our case, corresponds to $T^* \approx 3000\,\mathrm{K}$ (we assume that the energy is equally distributed between electrons and holes,[7]). For a given photon energy $\hbar\omega$, the values of E_a and E_b are uniquely defined on the basis of energy and momentum conservation:

$$E_a = -\left(\hbar\omega - E_g\right)\left(\frac{m_e}{m_e+m_h}\right) - E_g \quad \text{and} \quad E_b = \left(\hbar\omega - E_g\right)\left(\frac{m_h}{m_e+m_h}\right). \tag{S16}$$

The value of the carrier-dependent quasi-Fermi levels is computed by the Nilsson approximation:[8]

$$E^*_{F_v} = -\left[\ln\left(\frac{n_{fc}}{2N_v}\right) + \frac{n_{fc}}{2N_v}\left[64 + 0.05524 \cdot \frac{n_{fc}}{2N_v} \cdot \left(64 + \sqrt{\frac{n_{fc}}{2N_v}}\right)\right]^{-1/4}\right] k_B T^* - E_g^0 \quad \text{(S17)}$$

and

$$E^*_{F_c} = \left[\ln\left(\frac{n_{fc}}{2N_c}\right) + \frac{n_{fc}}{2N_c}\left[64 + 0.05524 \cdot \frac{n_{fc}}{2N_c} \cdot \left(64 + \sqrt{\frac{n_{fc}}{2N_c}}\right)\right]^{-1/4}\right] k_B T^*, \quad \text{(S18)}$$

where the *zero* energy level is set at the bottom of the conduction band. N_v and N_c are the effective density of states in the valence and conduction band, respectively, given by

$$N_v = 2\left(\frac{m_h\, k_B\, T^*}{2\pi\hbar}\right)^{3/2} \quad \text{and} \quad N_c = 2\left(\frac{m_e\, k_B\, T^*}{2\pi\hbar}\right)^{3/2}. \quad \text{(S19)}$$

The refractive index variation due to bandgap renormalization and band filling is obtained after the application of the Kramers-Krönig relations (see Eq. S8). The possible photoinduced variation of interband transitions at high energies, *i.e.* beyond the experimental accessible energy range, would gives rise to an additional refractive index variation, which is not accounted for by Eq. S14. This contribution is considered by assuming an additional frequency independent refractive index variation, δn_0, which can be adjusted to finely match the ratio between the amplitudes of the $\delta T/T$ signals at the energy $\hbar\omega \simeq$2.4 eV for the 150 nm and 300 nm NPs.

S6 Mie-theory of single particle

S6.1 Extinction, Scattering, and Absorption

In order to clarify how scattering and absorption mechanisms contribute to total extinction, we analytically calculated the scattering, extinction and absorption cross-sections (C_{sca}, C_{ext}, and C_{abs}, respectively) of a single sperical $CsPbBr_3$ particle, within the framework of Mie theory.[9] This model applies to the ideal case of isolated nanoparticles in a surrounding medium, but it is instructive to qualitatively address the role of the scattering and absorption processes. The analytical expressions are given by:

$$C_{\mathrm{sca}} = \frac{2\pi}{\mathrm{k}^2} \sum_{h=1}^{\infty} (2h+1)\ (|a_h|^2 + |b_h|^2) \tag{S20a}$$

$$C_{\mathrm{ext}} = \frac{2\pi}{\mathrm{k}^2} \sum_{h=1}^{\infty} (2h+1)\ \Re(a_h + b_h) \tag{S20b}$$

$$C_{\mathrm{abs}} = C_{\mathrm{ext}} - C_{\mathrm{sca}} \tag{S20c}$$

where the index h is the multipole order, a_h and b_h are the *scattering Mie-coefficients* of the order h, $\mathrm{k}=\frac{2\pi\sqrt{\varepsilon_{\mathrm{m}}}}{\lambda_0}$ is the wave-number in the surrounding medium, ε_{m} is the dielectric function of the surrounding medium, and λ_0 is the wavelength in vacuum. Assuming that the permeability of the particle equals to that of the surrounding medium, *Mie coefficients* can be obtained thanks to the following expressions:

$$a_h = \frac{m\psi_h(mx)\psi_h'(x) - \psi_h(x)\psi_h'(mx)}{m\psi_h(mx)\xi_h'(x) - \xi_h(x)\psi_h'(mx)} \tag{S21a}$$

$$b_h = \frac{\psi_h(mx)\psi_h'(x) - m\psi_h(x)\psi_h'(mx)}{\psi_h(mx)\xi_h'(x) - m\xi_h(x)\psi_h'(mx)}, \tag{S21b}$$

where ψ and ξ are the Riccati - Bessel functions, $m = \sqrt{\varepsilon_{\mathrm{np}}}/\sqrt{\varepsilon_{\mathrm{m}}}$ is the relative refractive index, $\varepsilon_{\mathrm{np}}$ is the dielectric function of the nanoparticle, $x = \pi\phi\sqrt{\varepsilon_{\mathrm{m}}}/\lambda_0$ is the size parameter, and ϕ is the sphere diameter. Basing on these equations and assuming that the dielectric

function of a $CsPbBr_3$ nanoparticle equals that of the thin film of the same material (extracted from Ref. 2), we calculate the cross-sections of the $CsPbBr_3$ spherical NPs with diameter of 150 and 300 nm (see Fig. S4). In both cases, near the exciton region, the scattering, characterized by a Fano asymmetric lineshape, dominates the total extinction.

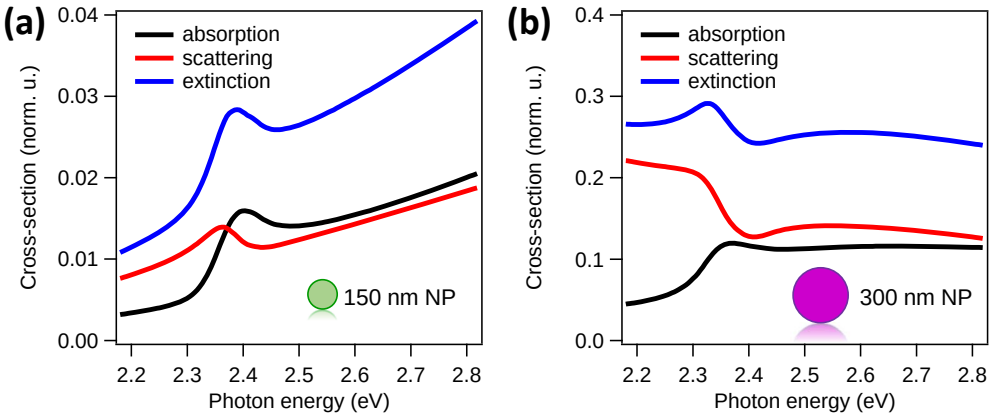

Figure S4: **Cross Sections for spherical $CsPbBr_3$ nanoparticles.** Extinction, scattering and absorption cross-sections of spherical $CsPbBr_3$ nanoparticles with diameter of 150 (panel a) and 300 nm (panel b) at equilibrium.

S6.2 Modes Decomposition (equilibrium and out-of-equilibrium)

In this section we describe how multipole decomposition of the scattering cross-section is spectrally modified by the photo-excitation process in the simple case of an isolated nanoparticle in a surrounding medium. The outcome of numerical simulations of the full electromagnetic problem in the realistic configuration (nanoparticle+substrate) is discussed in the main text. In expression S20, a_h (*electric*) and b_h (*magnetic*) are the Mie-coefficients of the order h. The multipole modes are named according to the order: h=1 stands for dipole mode, 2-quadrupole, 3-octupole, *etc.* Fig. S5a and c exhibit the scattering cross-section at equilibrium (obtained as described in S6.1), together with the contribution provided by the four strongest multipole modes (dipolar (D) and quadrupolar (Q) modes of magnetic (M) and electric (E) types), for a $CsPbBr_3$ particle with diameter of 150 and 300 nm (panel (a) and (c), respectively). The out-of-equilibrium scattering cross-section (*i.e.*, after photo-

excitation) is calculated thanks to expressions S20a, S21 by using a perturbed perovskite dispersion, $\varepsilon_{\text{out}} = \varepsilon_{\text{np}} + \delta\varepsilon_{\text{np}}$. The photo-induced variation of the nanoparticles dispersion $\delta\varepsilon_{\text{np}}$ is obtained as described in Sec. S5. The out-of-equilibrium cross-section, together with the contribution provided by the four strongest multipole modes, are reported in panels (b) and (d) for a $CsPbBr_3$ particle with diameter of 150 and 300 nm, respectively.

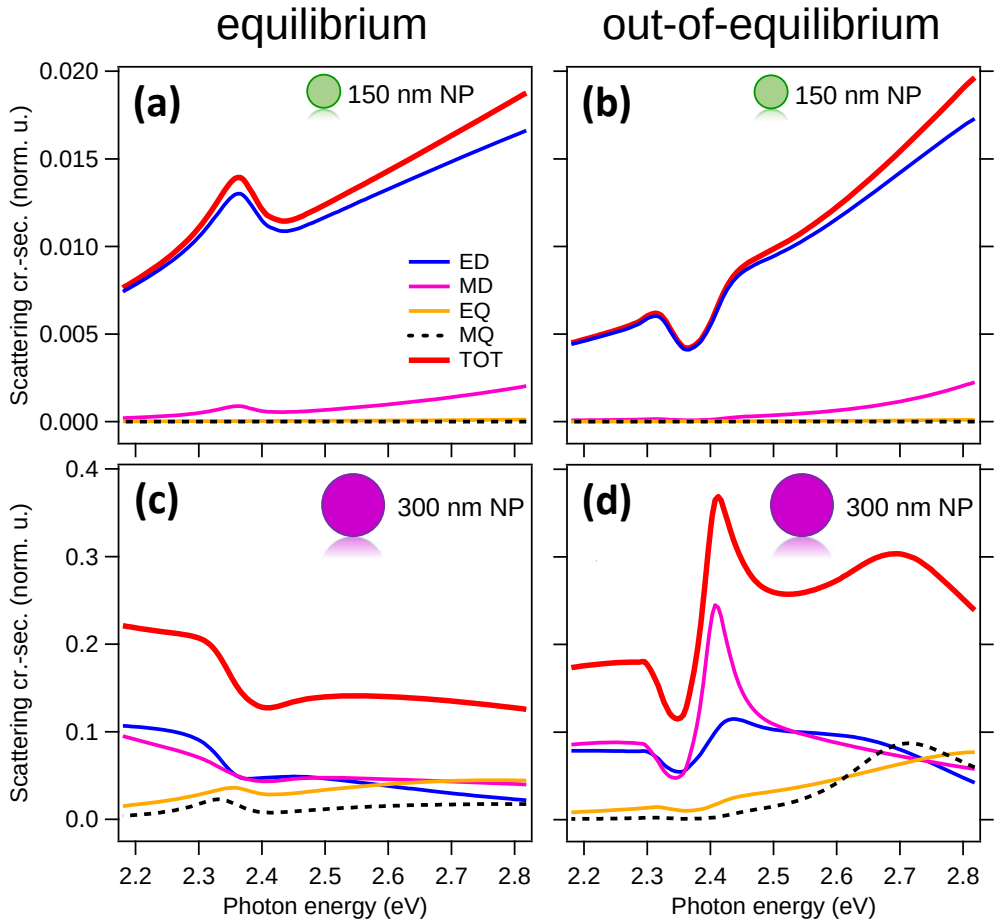

Figure S5: **Modes decomposition for spherical $CsPbBr_3$ nanoparticles.** Calculated scattering cross-section (red solid lines) for a spherical $CsPbBr_3$ nanoparticle of diameters 150 nm (a, b) and 300 nm (c, d), as well as contributions to the four strongest Mie modes in visible spectral range: electric dipole (ED, blue solid lines), magnetic dipole (MD, magenta solid lines), electric quadrupole (EQ, yellow solid lines), and magnetic quadrupole (MQ, black dashed lines). The spectra are calculated for unperturbed material before photo-excitation (a, c), and after photo-excitation assuming an injected free carrier density $n_{fc} = 1.2 \times 10^{20}\,\text{cm}^{-3}$ (b, d).

References

1. Battie, Y.; Resano-Garcia, A.; Chaoui, N.; Zhang, Y.; En Naciri, A. Extended Maxwell-Garnett-Mie Formulation Applied to Size Dispersion of Metallic Nanoparticles Embedded in Host Liquid Matrix. *J. Chem. Phys.* **2014**, *140*, 044705.

2. Tiguntseva, E. Y.; Baranov, D. G.; Pushkarev, A. P.; Munkhbat, B.; Komissarenko, F.; Franckevicius, M.; Zakhidov, A. A.; Shegai, T.; Kivshar, Y. S.; Makarov, S. V. Tunable Hybrid Fano Resonances in Halide Perovskite Nanoparticles. *Nano Lett.* **2018**, *18*, 5522–5529.

3. Bennett, B. R.; Soref, R. A.; Del Alamo, J. A. Carrier-Induced Change in Refractive Index of InP, GaAs and InGaAsP. *IEEE J. Quantum Electron.* **1990**, *26*, 113–122.

4. Stern, F. Dispersion of the Index of Refraction near the Absorption Edge of Semiconductors. *Phys. Rev.* **1964**, *133*, A1653–A1664.

5. Protesescu, L.; Yakunin, S.; Bodnarchuk, M. I.; Krieg, F.; Caputo, R.; Hendon, C. H.; Yang, R. X.; Walsh, A.; Kovalenko, M. V. Nanocrystals of Cesium Lead Halide Perovskites ($CsPbX_3$, X = Cl, Br and I): Novel Optoelectronic Materials Showing Bright Emission with Wide Color Gamut. *Nano Lett.* **2015**, *15*, 3692–3696.

6. Ahmad, M.; Rehman, G.; Ali, L.; Shafiq, M.; Iqbal, R.; Ahmad, R.; Khan, T.; Jalali-Asadabadi, S.; Maqbool, M.; Ahmad, I. Structural, Electronic and Optical Properties of $CsPbX_3$ (X = Cl, Br, I) for Energy Storage and Hybrid Solar Cell Applications. *J. Alloy Compd.* **2017**, *705*, 828 – 839.

7. Yang, Y.; Ostrowski, D. P.; France, R. M.; Zhu, K.; van de Lagemaat, J.; Luther, J. M.; Beard, M. C. Observation of a Hot-Phonon Bottleneck in Lead-Iodide Perovskites. *Nat. Photonics* **2015**, *10*, 53–59.

8. Nilsson, N. G. Empirical Approximations for the Fermi Energy in a Semiconductor with Parabolic Bands. *Appl. Phys. Lett.* **1978**, *33*, 653–654.

9. Bohren, C. F.; Huffman, D. R. *Absorption and Scattering of Light by Small Particles*, 1st ed.; John Wiley & Sons: New York, 1983.